Magazine of Concrete Research, 2007, **59**, No. 10, December, 743–756
doi: 10.1680/macr.2007.59.10.743

Propagation of flexural and shear cracks through reinforced concrete beams by the bridged crack model

A. Carpinteri*, J. R. Carmona† and G. Ventura*

Politecnico di Torino; Universidad de Castilla La Mancha

The bridged crack model has been developed for modelling the flexural behaviour of reinforced concrete beams and related size effects explaining brittle–ductile–brittle failure mode transitions. In the present paper the model is extended to analyse shear cracks, introducing a given shape for the hypothetical crack trajectory and determining the initial crack position and the load plotted against crack length curve for three-point bending problems. The proposed formulation reproduces the pure mode I flexural behaviour as a particular case, so that the flexural and the diagonal tension (shear) failure modes can be immediately compared to detect which one dominates and to determine the relevant failure load. The model can predict all the mutual transitions between the different collapse mechanisms. In the current paper these transitions are shown by varying the governing non-dimensional parameters.

Notation

A_s bar cross-section area
a crack depth
b beam width
c reinforcement cover
E concrete Young's modulus
F external load
h beam height
K_I stress-intensity factor at the crack tip
K_{IC} concrete toughness
K_{IP} stress-intensity factor owing to the closing force at the reinforcement bars
K_{IV} stress-intensity factor associated to the shear force
l shear span
N_P brittleness number for bending of reinforced concrete beams
P reinforcement reaction
P_P maximum for the bridging reinforcement reaction
V applied shear force
V_F shear for crack propagation
$\tilde{V}_F$ non-dimensional shear of crack propagation
V_P shear force of plastic flow or slippage
x horizontal distance from the support to the crack tip
x_0 initial crack mouth position
Y_M shape function for the determination of the stress-intensity factor due to an applied bending moment
Y_P shape function for the determination of the stress-intensity factor due to a couple of concentrated forces applied on the crack faces
α non-dimensional horizontal distance from the support to the crack tip
α_0 non-dimensional initial crack mouth position
Γ crack trajectory
γ trajectory angle
ζ non-dimensional reinforcement cover
λ_l shear span slenderness ratio
μ trajectory exponent
υ displacement of the point of application of the external load
ξ non-dimensional crack depth
ρ reinforcement area percentage
σ_s bar traction
σ_y minimum between the yielding and sliding stress for the bars
ω crack opening at the reinforcement level

* Department of Structural and Geothecnical Engineering, Politecnico di Torino, Corso Duca degli Abruzzi, 24, 10129, Torino, Italy
† E.T.S. de ingenieros de Caminos, Canales y Puertos, Universidad de Castilla La Mancha, 13071, Ciudad Real, Spain

(MCR 61591) Paper received 7 August 2006; last revised 4 May 2007; accepted 9 July 2007

www.concrete-research.com 1751-763X (Online) 0024-9831 (Print)

Introduction

In reinforced concrete (RC) elements of ordinary dimensions without stirrups, with a slenderness ratio up to 5, subject to three-point bending, the first cracks usually form close to the region of maximum bending moment. As the load increases, more cracks may be formed away from the region of maximum moment. These cracks also start as bending cracks, approximately normal to the axis of the beam. Under a further increase in loading, cracks located along the shear span grow oriented normally to the major tensile principal stress. As these cracks are formed in regions where the shearing force is no longer small, they grow in the presence of combined tension and shear stresses. These cracks are commonly called 'shear cracks'. As the external load increases, one of the shear cracks usually propagates unstably, leading to the failure of the beam. This kind of collapse is described in short as diagonal tension (shear) failure. Nevertheless, depending on geometrical characteristics and material properties, failure owing to reinforcement yielding (flexural failure) may occur before diagonal tension failure, if the element does not fail owing to a crack initiation.[1–3]

The transitions between flexural and diagonal tension failures in RC elements—inside a consistent theoretical framework—have represented an unsolved problem for some considerable time. The main aim of the present analysis is to obtain a consistent modelling of the shear crack's behaviour and diagonal tension failure. The problem of shear failure as a consequence of crack propagation remains unresolved, despite numerous extensive studies over the last 50 years. The significant current interest in this area is reflected by the large number of recent studies in this field. As shear failure takes place through a cracking process, it appears appropriate to study the problem using fracture mechanics theories. The main advantage of using fracture mechanics rather than other theories, for example based on strut-and-tie models[4] or the compression field approach,[5,6] is the existence of a sound base theory which is able to study the connection between the cracking process in the RC element and the failure load.

In the field of fracture mechanics and using a cohesive model to describe concrete behaviour, some analyses have been performed by Gustafsson,[7] Gustafsson and Hillerborg[8] and Niwa[9,10] among others. In the framework of linear elastic fracture mechanics, and in order to avoid finite-element computations, some models are particularly prominent in the current paper's list of references, which is aimed at finding a rational interpretation of the diagonal tension failure mode. In particular, Jenq and Shah[11] analysed the diagonal shear fracture superposing the contribution of concrete and steel bars, with a technique that is somehow conceptually close to the bridged crack model.[2] The reinforcement force is computed from the classical no-tension strength calculation and the element load capacity is evaluated from the stress-intensity factor at the crack tip. Some further developments of this work with other original contributions were given by So and Karihaloo.[12,13] More recently, the problem has been studied in the framework of fracture mechanics by, among others, Gastebled and May,[14] who assumed that the failure is attributable to a rotation about the crack tip of the diagonal crack triggered by concrete splitting at the steel bars.

The bridged crack model was originally proposed by Carpinteri[1,2] for the study of RC beams by fracture mechanics. The problem of the size effect and the brittle–ductile transition were analysed with reference to the problem of minimum reinforcement.[15,16] Subsequently, the action of cohesive stresses has been introduced in addition to that of the reinforcing bars.[17]

In the present work, the behaviour of RC beams without stirrups is analysed, using the bridged crack model. To extend the model and account for the shear crack's behaviour and evaluate diagonal tension failure load, some additional hypotheses are introduced. In particular, the crack trajectory is given by an assumed analytical law based on experimental observations. Comparing the different load plotted against crack length curves for each crack trajectory, a criterion to evaluate diagonal tension failure is obtained. A second assumption concerns the evaluation of the stress-intensity factors. It is assumed that the crack propagates only in mode I, and an approximate analytical expression for the stress-intensity factors is given. This assumption has been validated by computing the stress-intensity factors numerically through the boundary element code developed by Portela and Aliabadi.[18] When the starting-point abscissa of the crack trajectory is at the beam midspan, the model naturally coincides with the traditional bridged crack model for the pure flexural problem. In this way, the different collapse modes are joined together into a unified general model, so that the simulation of the transitional phenomena is naturally accomplished. The model is analysed considering the influence of the variation in the non-dimensional parameters on the mechanical response of the RC element and the related failure mode transitions. A rational explanation is also given to the problem of diagonal tension failure.

Basic assumptions

RC elements have a complex crack pattern depending on the geometry of the structural element, the reinforcement percentage, the steel–concrete bond condition and the local defects of the concrete itself. As mentioned in the Introduction, in three-point bending tests the diagonal tension failure usually develops by forming a series of stable shear cracks originating along the shear span, initially with vertical direction and then extending towards the point-load zone. If

diagonal tension failure is the dominant mechanism, an unstable crack takes place, unloading all the previously formed cracks and bringing the beam to collapse (Fig. 1). This crack will hereafter be referred to as the 'critical crack'. This critical crack is usually accompanied by a secondary crack, horizontal and approximately at the reinforcement layer level. This sequence suggests that it is not inappropriate to consider the critical crack as isolated, with no interaction with the previously formed stable cracks.

Attention is therefore focused on modelling a single, isolated crack, by assuming the crack length as a monotonically increasing control parameter. It will be furthermore assumed that no stirrups are present. Dowel action and aggregate interlock will be neglected and the steel reinforcing bars will be considered as rigid-perfectly plastic. In beams without shear reinforcement, it should be noted that, before the failure, most of the load is carried by the concrete ligament above the tip of the crack. At failure the shear is transferred to the bars owing to the loss of stiffness of the concrete ligament, and the dowel action generates a horizontal, longitudinal crack at the reinforcement level.[19] The absence of shear reinforcement allows the dowel action to be neglected, since the load carried by this mechanism is small. Similarly, regarding aggregate interlock, this effect does not have a significant influence on the maximum load in beams without stirrups.[20,21] It is observed that, just before failure, compression stresses are more or less parallel to the end portion of crack, so that shear stresses owing to aggregate interlock cannot have a significant effect on the failure load.

In all cases, the above assumptions imply that the calculated shear strengths are conservative. Linear elastic fracture mechanics will be considered in the following, so that the stress-intensity factor at the crack tip can be evaluated by linear superposition of the effects of the external loading and of the reinforcement reaction, Fig. 2. All these hypotheses are typical of the bridged crack model.

Two additional hypotheses are then considered: the shape of the crack trajectory and a simplified evaluation of the stress-intensity factors. These will be detailed in the following sections.

Crack trajectory

In ordinary three-point bending beams without shear reinforcement, cracks present a typical shape. The first crack usually takes place by flexure, is approximately at the midspan and is perpendicular to the lower edge of the beam. As the load is increased, the crack grows towards the point-load and, at the same time, other cracks usually develop along the beam span (unless reinforcement percentage or shear bonding strength are very low). These originate from points along the lower edge and then, as they propagate, their trajectories curve towards the applied load. A typical crack path is shown in Fig. 3, where some geometrical quantities used in the following developments are defined.

The crack trajectory Γ is considered to comprise two parts. A first segment Γ_1 is vertical and extends from the bottom to the reinforcement layer. The second part Γ_2 is assumed to be a power law with some given exponent, extending from the end of the first part to the load point. The crack trajectory $\Gamma = \Gamma_1 \bigcup \Gamma_2$ is defined analytically by

$$\Gamma(a) = \begin{cases} x_0 & c \geqslant a \\ x_0 + \left(\dfrac{a-c}{h-c}\right)^{\mu} (l - x_0) & c \leqslant a \leqslant h \end{cases} \quad (1)$$

where h is the beam depth, l is the shear span, a is the crack depth, c is the reinforcement cover, x is the crack tip horizontal position, x_0 is the crack mouth horizontal

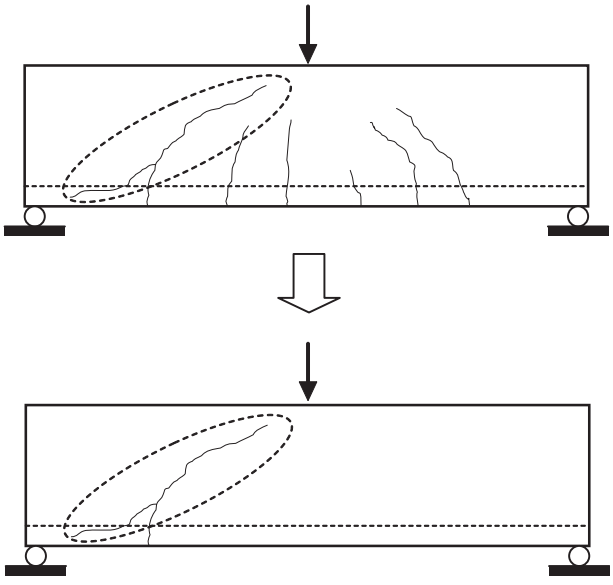

Fig. 1. Diagonal tension failure by the formation of a dominant, unstable shear crack

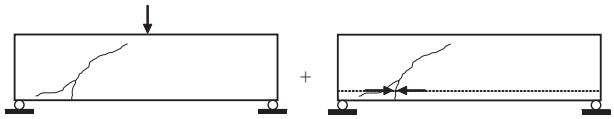

Fig. 2. Evaluation of the stress-intensity factors by linear superposition

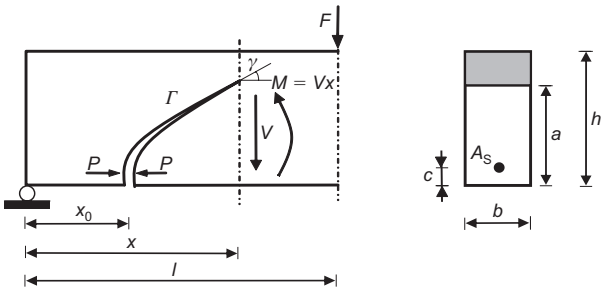

Fig. 3. Cracked beam element

position and μ is the exponent of the crack trajectory function.

The crack trajectory, equation (1), can be conveniently cast in non-dimensional form. Let

$$\alpha_0 = \frac{x_0}{l}; \quad \alpha = \frac{x}{l}; \quad \xi = \frac{a}{h}; \quad \zeta = \frac{c}{h}; \quad \lambda_l = \frac{l}{h} \tag{2}$$

Introducing the ratios of equation (2) into equation (1)

$$\alpha(\zeta, \xi) = \begin{cases} \alpha_0 & \zeta \geqslant \xi \\ \alpha_0 + \left(\dfrac{\xi - \zeta}{1 - \zeta}\right)^{\mu} (1 - \alpha_0) & \zeta \leqslant \xi \leqslant 1 \end{cases} \tag{3}$$

where α is the non-dimensional horizontal distance of the crack tip from the support, ξ is the crack depth, α_0 is the initial crack mouth position and ζ is the reinforcement depth. All these non-dimensional parameters range from 0 to 1.

Some crack trajectories are drawn in Fig. 4, assuming different exponents and two slenderness ratios λ_l, defined as the ratio between the shear span and the beam depth, equation (2). The trajectories are represented in the non-dimensional plane, although the axes have been scaled depending on the ratio λ_l.

Stress-intensity factors

Until now, neither closed-form solutions nor non-linear regressions of numerical data have been given for the evaluation of the stress-intensity factors, that is for the geometry given in Fig. 2 and the crack trajectory shown in Fig. 3. In particular, according to the superposition principle illustrated in Fig. 2, the stress-intensity factor evaluation is required in the cases of (*a*) external load and (*b*) reaction of the reinforcement.

To evaluate the stress-intensity factor owing to the external load, Jenq and Shah[11] assumed that it can be approximated by the stress-intensity factor of a bent beam with a symmetric edge notch of depth *a* subjected to the bending moment corresponding to the cross-section at the mouth of the crack. Here a similar approach is followed, but the variation of the bending moment at each section owing to the crack path will be accounted for. Karihaloo[12] introduced this idea in the model of Jenq and Shah.

The stress-intensity factor produced at the crack tip by an applied bending moment, M, is given by[22,23]

$$K_{IM} = \frac{M}{h^{3/2} b} Y_M(\xi) \tag{4}$$

where, with reference to Fig. 3, the bending moment at the crack tip is given by

$$M = Vx = Vl\alpha(\zeta, \xi) \tag{5}$$

with $\alpha(\zeta, \xi)$ given by equation (3).

Introducing equation (5) into equation (4) and rearranging, the stress-intensity factor is given by the form

$$K_{IV} = \frac{Vl\alpha(\zeta, \xi)}{h^{3/2} b} Y_M(\xi) = \frac{V\lambda_l}{h^{1/2} b} Y_V(\xi) \tag{6}$$

where

$$Y_V(\zeta, \xi) = \alpha(\zeta, \xi) Y_M(\xi) \tag{7}$$

This hypothesis is confirmed by some numerical boundary element calculations[18] to obtain the stress-intensity factor for different geometries and different positions of the crack tip. Fig. 5 shows some results which demonstrate that the approximation does not result in large errors, apart from very low ratios λ_l, where the beam model is inappropriate.

The stress-intensity factor produced at the crack tip by the forces P, applied at the level of reinforcement at a distance c from the lower edge of the beam, for a straight vertical crack is equal to

$$K_{IP} = \frac{P}{h^{3/2} b} Y_P(\zeta, \xi) \tag{8}$$

Function $Y_P(\zeta, \xi)$ is reported in the stress-intensity factors handbooks.[22] It will be assumed herein that the crack shape does not have a large influence on K_{IP}, and

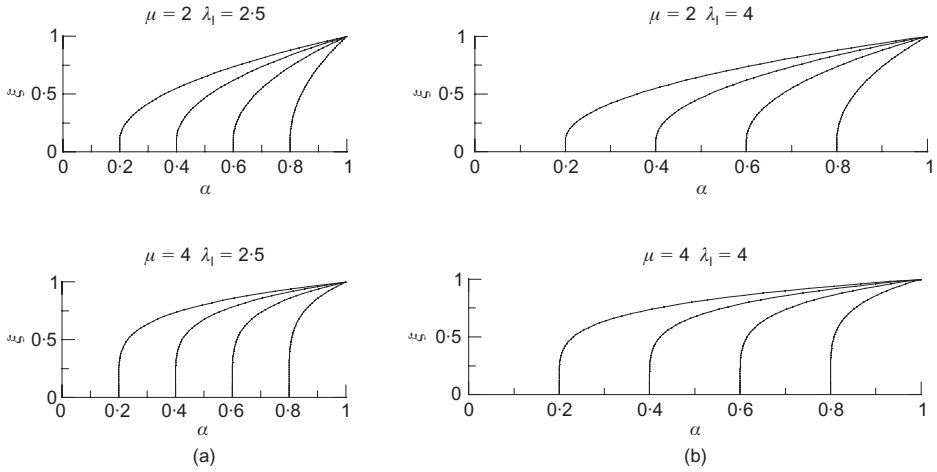

Fig.4. Normalised crack trajectories: (a) $\lambda_l = 2{\cdot}5$; (b) $\lambda_l = 4$

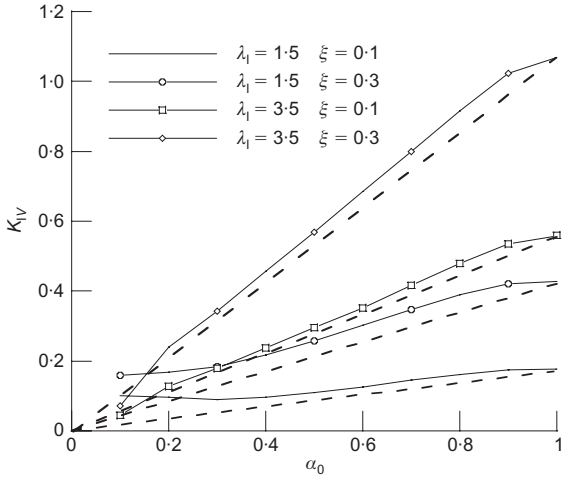

Fig. 5. Stress-intensity factors along shear span. Comparison of the boundary element results (light lines) to the approximation, equation (7) (dotted lines)

it is therefore considered to be a function only of the crack depth.

Several numerical analyses by boundary elements[18] have been made to obtain an approximation to the stress-intensity factor for different positions of the crack tip. It is observed that the stress-intensity factor is a function of the angle γ, Fig. 3. Consequently, a function $\beta(\gamma)$ to approximate the variation of $Y_P(\zeta, \xi)$ with γ has been defined as

$$\beta(\gamma) = \left(\frac{\gamma}{90}\right)^{0{\cdot}2} \tag{9}$$

where the angle γ is expressed in degrees. The shape function can be approximated as

$$Y_P^{\gamma}(\zeta, \xi) = Y_P(\zeta, \xi)\beta(\gamma) \tag{10}$$

Finally, the stress-intensity factor owing to the reinforcement reactions P is given by

$$K_{IP} = \frac{P}{h^{3/2}b} Y_P(\zeta, \xi)\beta(\gamma) = \frac{P}{h^{3/2}b} Y_P^{\gamma}(\zeta, \xi) \tag{11}$$

Fracture mechanics modelling of a reinforced concrete beam with a diagonal crack

Consider the cracked beam element shown in Fig. 3, which undergoes simultaneously the bending moment, function of the shearing force V and of the crack tip position abscissa x, and the reinforcement closing forces P applied on the crack faces. The development of a single crack is considered, with arbitrary location of the crack initiation point. This will allow the critical crack and the corresponding ultimate failure load to be determined.

The displacement Δv of the point of application of the external load F and the relative displacement $\Delta\omega$ of the points of application of the reinforcement reactions P can be expressed by linear superposition as the sum of a part owing to V and a part owing to P

$$\Delta v = \Delta v_{VV} + \Delta v_{VP} = \lambda_{VV} V - \lambda_{VP} P \tag{12}$$

$$\Delta\omega = \Delta\omega_{VV} + \Delta\omega_{VP} = \lambda_{PV} V - \lambda_{PP} P \tag{13}$$

where λ_{VV}, λ_{VP}, λ_{PV} and λ_{PP} are the compliances of the member owing to the existence of the crack. The factors λ can be derived from energy methods as follows. If G and E are, respectively, the strain energy release rate and the Young's modulus of the material (the Poisson ratio is considered as negligible), it follows that the variation ΔW of the total potential energy is given by

$$\begin{aligned}
\Delta W &= \int_{\Gamma} Gb\,\mathrm{d}\Gamma = \int_{\Gamma_1} G_V b\,\mathrm{d}\Gamma_1 + \int_{\Gamma_2} G_{(V+P)} b\,\mathrm{d}\Gamma_2 \\
&= \int_{\Gamma_1} \frac{K_{1V}^2}{E} b\,\mathrm{d}\Gamma_1 + \int_{\Gamma_2} \frac{(K_{1V} + K_{1P})^2}{E} b\,\mathrm{d}\Gamma_2 \\
&= \int_{\Gamma_1} \frac{K_{1V}^2}{E} b\,\mathrm{d}\Gamma_1 + \int_{\Gamma_2} \frac{K_{IV}^2}{E} b\,\mathrm{d}\Gamma_2 \\
&\quad + \int_{\Gamma_2} \frac{K_{1P}^2}{E} b\,\mathrm{d}\Gamma_2 + 2\int_{\Gamma_1} \frac{K_{IV} K_{1P}}{E} b\,\mathrm{d}\Gamma_2 \\
&= \int_{\Gamma} \frac{K_{1V}^2}{E} b\,\mathrm{d}\Gamma + \int_{\Gamma_2} \frac{K_{1P}^2}{E} b\,\mathrm{d}\Gamma_2 + 2\int_{\Gamma_1} \frac{K_{1V} K_{1P}}{E} b\,\mathrm{d}\Gamma_2
\end{aligned} \tag{14}$$

where K_{1V} and K_{1P} are the stress-intensity factors owing to shearing force V and to the reinforcement forces P, respectively. An application of Clapeyron's Theorem provides

$$\begin{aligned}
\Delta W = \frac{1}{2} V \Delta v_{VV} + \frac{1}{2} P \Delta\omega_{PP} \\
+ \frac{1}{2}(P\Delta\omega_{PV} + V\Delta v_{VP})
\end{aligned} \tag{15}$$

Recalling that according to Betti's Theorem $P\Delta\omega_{PV} = V\Delta v_{VP}$, from equations (12) to (15) and calling s the curvilinear abscissa along the crack trajectory (Γ), it follows that

$$\Delta v_{VV} = \lambda_{VV} V = \frac{2}{V} \int_{\Gamma} \frac{K_{1V}^2}{E} b\,\mathrm{d}s \tag{16}$$

$$\Delta\omega_{PP} = \lambda_{PP} P = \frac{2}{V} \int_{\Gamma_2} \frac{K_{1P}^2}{E} b\,\mathrm{d}s \tag{17}$$

$$\begin{aligned}
P\Delta\omega_{PV} = V\Delta v_{VP} = \lambda_{VP} P \\
= \lambda_{PV} V = \frac{2}{V} \int_{\Gamma_2} \frac{K_{1P} K_{1V}}{E} b\,\mathrm{d}s
\end{aligned} \tag{18}$$

The stress-intensity factor produced at the crack tip by the shear V is given by equation (6). Let $g(\zeta, \xi)$ the Jacobian mapping the curvilinear integral along the

crack trajectory onto the interval [0, ξ], so that the change of integral variable $ds = g(\zeta, \xi)dz$ can be introduced in the evaluation of the compliances. For the given crack trajectory, equation (3), $g(\zeta, \xi)$ is equal to

$$g(\zeta, \xi) = \begin{cases} 1 & z < \zeta \\ \sqrt{\mu^2 \lambda_l^2 \left(\dfrac{1}{1-\zeta}\right)^{2\mu}} & z \geqslant \zeta \\ \sqrt{(z-\zeta)^{2(\mu-1)}(1-\alpha_0)^2 + 1} & \end{cases} \quad (19)$$

Substituting equation (6) into equation (16), the compliance λ_{VV} (displacement produced by $V = 1$), can be expressed as

$$\lambda_{VV} = \frac{2\lambda_l^2}{Eb} \times \left[\int_0^{\xi} Y_V^2(z) g(\zeta, z)dz + \int_{\zeta}^{\xi} Y_V^2(z) g(\zeta, z)dz\right] \quad (20)$$

From equations (11) and (17), the compliance λ_{PP} (crack opening displacement produced by $P = 1$) is provided by

$$\lambda_{PP} = \frac{2}{Eb} \int_{\zeta}^{\xi} Y_V^{\gamma^2}(\zeta, z) g(\zeta, z)dz \quad (21)$$

Substituting equations (6) and (11) into equation (18) and dividing by the product VP, the mutual compliance $\lambda_{VP} = \lambda_{PV}$ can be expressed in the form

$$\lambda_{VP} = \lambda_{PV} = \frac{2\lambda_l}{Eb} \int_{\zeta}^{\xi} Y_P^{\gamma}(\zeta, z) Y_V(z) g(\zeta, z)dz \quad (22)$$

Evaluation of reinforcement reaction

Let σ_s and A_s be the reinforcement stress and cross-sectional area, respectively, related to the total reaction by $P = \sigma_s A_s$. The relative displacement in the cracked cross-section at the level of reinforcement is assumed to be zero up to the yielding or slippage of the reinforcement (rigid-plastic behaviour). The displacement compatibility condition $\Delta\omega = 0$ allows the unknown force P to be acquired as a function of the applied shear V. In fact, from equation (13)

$$\frac{P}{V} = \frac{\lambda_{PV}}{\lambda_{PP}} = \frac{1}{r''(\zeta, \xi)} \quad (23)$$

where

$$r''(\zeta, \xi) = \frac{\lambda_{PP}}{\lambda_{PV}} = \frac{\displaystyle\int_{\zeta}^{\xi} Y_V^{\gamma^2}(\zeta, z) g(\zeta, z)dz}{\lambda_l \displaystyle\int_{\zeta}^{\xi} Y_V^{\gamma}(\zeta, z) Y_V(z) g(\zeta, z)dz} \quad (24)$$

Considering a rigid-perfectly plastic behaviour of the reinforcement, the shearing force of plastic flow or slippage is obtained from equation (23)

$$V_P = P_P \frac{\lambda_{PP}}{\lambda_{PV}} = P_P r''(\zeta, \xi) \quad (25)$$

where $P_P = \sigma_y A_s$ indicates the yielding (or pulling-out) force, achieved when $\sigma_s = \sigma_y$ (yield or pulling-out strength of reinforcement).

Shearing force of incipient crack propagation

With reference to Fig. 3, let K_I be the stress-intensity factor at the crack tip. By the superposition principle, it is given by the sum of the stress-intensity factor K_{IV} owing to the bending moment associated to the shearing force and K_{IP}, owing to the closing forces at the reinforcement position

$$K_I = K_{IV} - K_{IP} \quad (26)$$

The crack propagation condition is ruled by the comparison of the stress-intensity factor K_I, equation (26), to the concrete fracture toughness K_{IC}

$$K_I = K_{IV} - K_{IP} = K_{IC} \quad (27)$$

The value of K_{IC} in equation (27) may be determined by the RILEM recommendations,[24,25] or derived by the procedures suggested in Refs 26 and 27 as $K_{IC} = (EG)^{0.5}$.

Moreover, let V_F be the shear for which $K_I = K_{IC}$. Introducing equations (6) and (11) into equation (26)

$$K_{IC} = \lambda_l \frac{V_F}{h^{1/2} b} Y_V(\xi) - \frac{P}{h^{1/2} b} Y_P^{\gamma}(\zeta, z) \quad (28)$$

and dividing both sides by K_{IC}

$$\frac{V_F}{K_{IC} h^{1/2} b} = \frac{1}{\lambda_l Y_V(\xi)} \left[1 + \frac{P}{K_{IC} h^{1/2} b} Y_P^{\gamma}(\zeta, z)\right] \quad (29)$$

Let $A = bh$ be the area of the cross-section and $\rho = A_s/A$ the reinforcement percentage. Consider the following brittleness number[2]

$$N_P = \frac{\sigma_y h^{1/2}}{K_{IC}} \rho \quad (30)$$

If the force transmitted by the reinforcement is equal to $P_P = \sigma_y A_s$, in other words, if the reinforcement traction limit has already been reached ($V_F \geqslant V_P$), then

$$\frac{V_F}{K_{IC} h^{1/2} b} = \frac{1}{\lambda_l Y_V(\xi)} \left[1 + N_P Y_P^{\gamma}(\zeta, z)\right] \quad (31)$$

In the case $V_F < V_P$, the reinforcement is in the elastic range, and the following relation holds

$$\frac{V_F}{K_{IC}h^{1/2}b} = \frac{1}{\lambda_l Y_V(\xi)}\left[1 + N_P\frac{\sigma_s}{\sigma_y}Y_P^{\gamma}(\zeta, z)\right] \quad (32)$$

or, equivalently

$$\frac{V_F}{K_{IC}h^{1/2}b} = \frac{1}{\lambda_l\{Y_V(\xi) - [Y_P^{\gamma}(\zeta, z)\lambda_{PV}/\lambda_{PP}]\}} \quad (33)$$

where the left-hand side represents the non-dimensional shearing force $\tilde{V}_F$

$$\tilde{V}_F = \frac{V_F}{K_{IC}h^{1/2}b} \quad (34)$$

Therefore, according to the model, when $V_F < V_P$, the shear force of crack propagation V_F depends only on the relative crack depth ξ, and is not affected by the brittleness number N_P—that is, it does not depend on the reinforcement percentage or beam depth but only on its relative crack depth ξ. For an easier understanding of the model, it is assumed in the present paper that the exponent μ, which defines the crack trajectory, is independent of the non-dimensional parameters N_P and λ_l. This hypothesis does not impair the generality of the approach. The possible dependence of the exponent μ on the brittleness number N_P and on the shear span-to-depth slenderness ratio λ_l is being developed both theoretically and by studying the results of experimental tests.

Model response to the variation of the non-dimensional parameters

Influence of the initial crack position

In this section it will be shown how the value of the initial crack position α_0 affects the mechanical response of the beam and implies the stability/instability of the cracking process. For the sake of clarity, reference is made to a real example, based on experimental results. The experimental test was performed by Bosco *et al.*,[28] and it was identified as B100–06. The material properties and beam geometry are shown in Fig. 6.

The following non-dimensional parameters characterise the simulation case: $\lambda_l = 2{\cdot}5$, $\zeta = 0{\cdot}1$, $N_P = 1{\cdot}41$. Moreover, a constant reinforcement is assumed along the span and a fourth-order crack trajectory curve ($\mu = 4$). Figs 6(b) to (d) show the non-dimensional shearing force plotted against crack depth curves for the initial crack position α_0 in the interval (0·3, 1·0), as well as the considered crack trajectory.

It is well known that the crack growth may present stable or unstable behaviour. When the crack growth is stable, an increase in the crack depth requires a load increase to fulfil the model equations. Conversely, unstable crack growth requires a load decrease. Both kinds of behaviour can occur at different load levels during crack propagation, see Figs 6(b), (c) and (d).

When the initial crack position is at the midspan ($\alpha_0 = 1{\cdot}0$), Fig. 6(b), the model coincides with the original bridged crack for beams in flexure (no shear). Immediately after the crack crosses the reinforcement, an unstable branch begins. This turns stable for a crack depth $\xi \approx 0{\cdot}3$. Then the non-dimensional shearing force grows until the yielding of steel takes place ($\xi \approx 0{\cdot}7$).

The second plot, Fig. 6(c), computed for an initial crack position $\alpha_0 = 0{\cdot}70$, shows the same characteristic behaviour for low values of the crack depth, followed by an unstable process before the steel yielding takes place. In fact, in this case, for a crack depth $\xi \approx 0{\cdot}65$ the type of propagation changes and an unstable crack branch begins up to the beam failure. In this case, as for the flexural crack originating at $\alpha_0 = 1{\cdot}0$, the reinforcement reaction stabilises the crack propagation for low crack depths but there is a point where the crack changes the type of propagation and the reinforcement is no longer able to stabilise its propagation. The change in the nature of the propagation provokes the relative maximum observed in Fig. 6(c). This change in the nature of crack propagation for a shear crack in RC beams without stirrups has been reported experimentally by Carmona.[29] Experimental results show that, after the maximum load and during the unstable crack growth, there exists a redistribution of the shear-carrying capacity from the concrete ligament to the steel bars by dowel action. The concrete surrounding the reinforcement is not able to withstand the load transmitted by the bars and then a longitudinal crack at the reinforcement level commences. This secondary effect occurs after the maximum load is outside the capability of the model.

For an initial crack position closer to the support, Fig. 6(d) ($\alpha_0 = 0{\cdot}3$), the maximum separating stable and unstable branches of the cracking process disappear and a completely unstable behaviour is observed. In this case, the reinforcement reaction is not able to stabilise the crack propagation throughout the entire process and the beam fails immediately after crack initiation. In this sense, it can be shown that a crack presents increasingly unstable behaviour when its initial point approaches the support. The other limiting case is represented by a crack with its initial point at the midspan (flexural crack), where, provided the reinforcement percentage is not too low, it is impossible to develop an unstable cracking process once the reinforcement reaction stabilises the initial instability ($\xi \geqslant 0{\cdot}3$).

The beam is assumed to be precracked throughout its length. Neglecting the singularity at the reinforcement depth ($\xi = 0{\cdot}1$), as the shear $\tilde{V}_F$ is increased, the first crack curve to be intersected is the one corresponding to the initial crack position $\alpha_0 = 1{\cdot}0$—that is, the beam midspan. Therefore, the first crack to become active is the one at the midspan and, if the load is slightly increased, its propagation is stable, since the curve ξ plotted against $\tilde{V}_F$ increases. This is represented in Fig. 7(a). The dashed horizontal line represents the load level and the curve is the crack propagation curve for $\alpha_0 = 1{\cdot}0$, as it appears from the symbols in the legend.

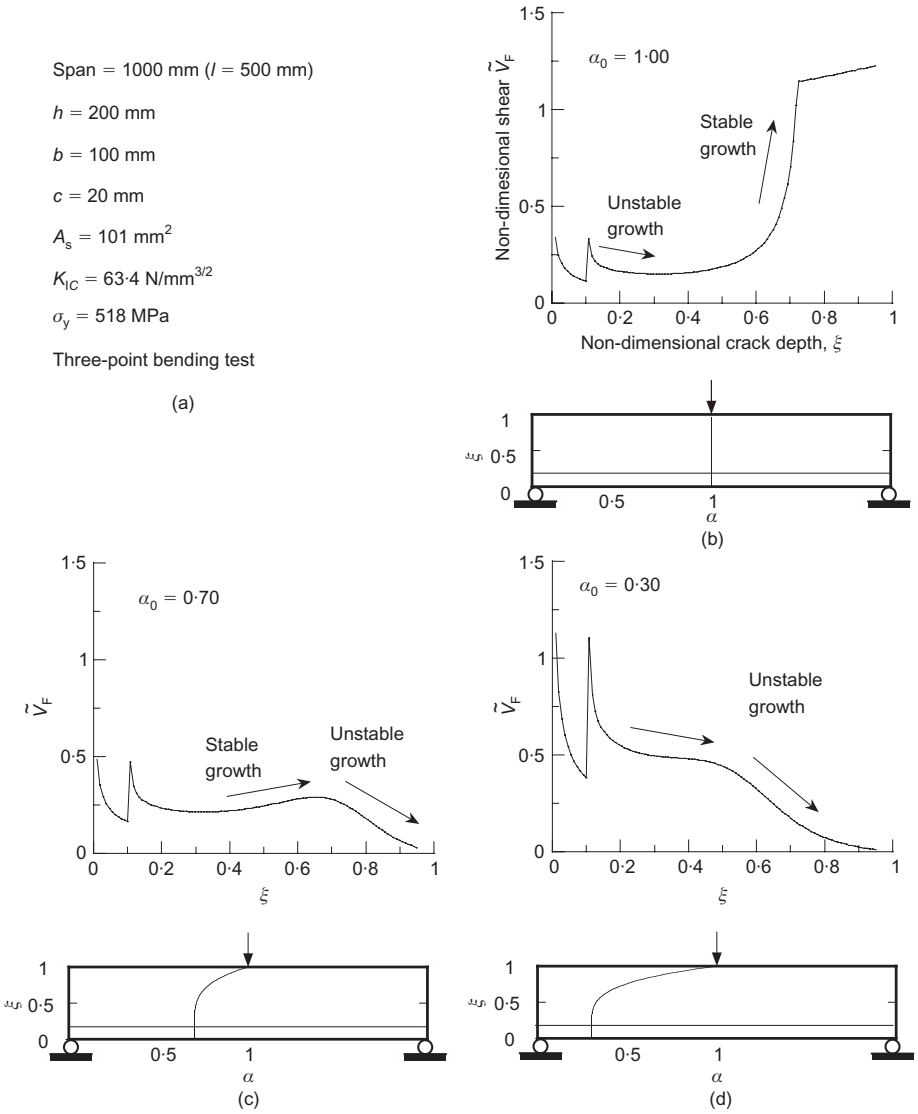

Fig. 6. Non-dimensional shearing force plotted against crack depth: (a) material properties and beam geometry; (b) initial crack position $\alpha_0 = 1{\cdot}00$; (c) initial crack position $\alpha_0 = 0{\cdot}70$; (d) initial crack position $\alpha_0 = 0{\cdot}30$

The sketch of the beam beneath the plot shows that the only active crack is at the midspan and its actual depth.

As the shear increases, Fig. 7(b), more crack propagation curves become active at the new load level. The cracking process develops along the marked curve segments of Fig. 7(b), so that the cracks with initial positions $\alpha_0 = 1{\cdot}0$, $0{\cdot}9$, $0{\cdot}8$ are now active and have different depths; see the beam sketched at the bottom of Fig. 7(b). In the same way, Fig. 7(c) illustrates the cracking process with a further increase of the external load. It can be seen that all the cracks activated up to this point are stable.

Consider finally Fig. 7(d). As the load is increased, the curve for $\alpha_0 = 0{\cdot}6$ is intersected, and the relevant crack starts to propagate. Let us observe, however, that the shear can be increased up to the level indicated by the dashed line, tangent to the maximum point of the curve for $\alpha_0 = 0{\cdot}6$. As the load reaches this level, the cracking process turns suddenly unstable because of the descending branch of the curve for $\alpha_0 = 0{\cdot}6$. In this way the model determines the shear at failure and the failure crack pattern.

In the example shown in Fig. 7(d), the critical crack is obtained for an initial position equal to $\alpha_0 = 0{\cdot}6$ and a crack depth $\xi = 0{\cdot}62$. The non-dimensional shearing force at failure has a value of $\tilde{V}_F = 0{\cdot}29$. Physically, this value represents the minimum load for which an unstable process can develop bringing the beam to failure. The obtained qualitative behaviour of shear crack propagation is similar to most of the descriptions of diagonal tension failure found in the literature. Note that the completely unstable cracks originating close to the support (e.g. $\alpha_0 < 0{\cdot}5$) cannot activate as they would need a much higher shearing force or a very deep initial crack.

Figure 8(a) shows a superposition of the plots for several initial crack positions. Observe that, neglecting the singularity at the reinforcement position, each curve

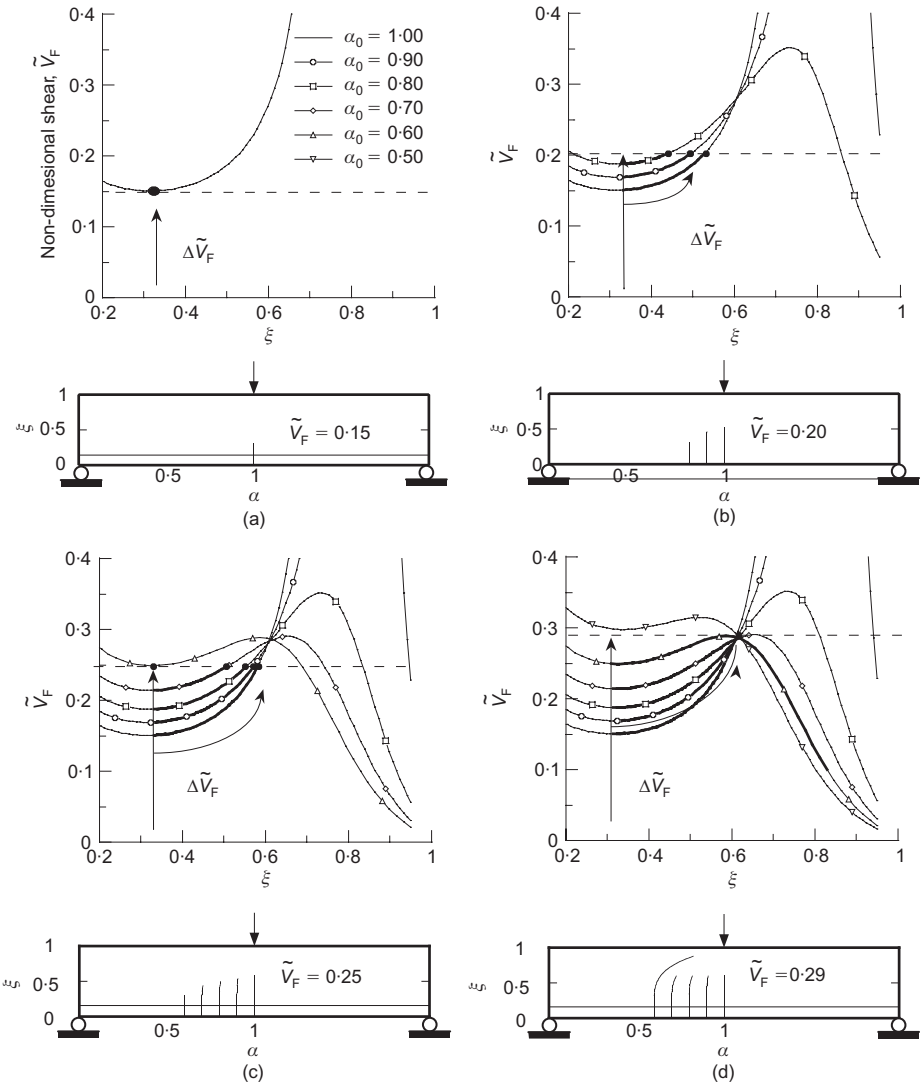

Fig. 7. Crack propagation process with a monotonically increasing load. $\tilde{V}_F$ plotted against ξ curves and cracks pattern for: (a) $\tilde{V}_F = 0{\cdot}15$; (b) $\tilde{V}_F = 0{\cdot}20$; (c) $\tilde{V}_F = 0{\cdot}25$; (d) $\tilde{V}_F = 0{\cdot}29$

presents a relative maximum with the exception of cracks near the support, which are unstable throughout all the propagation process. The thick line in Fig. 8(b) represents the crack having the property that its relative maximum is minimum among the maxima. In the following this crack will be referred to as the critical crack, as it represents the cracking process corresponding to the minimum required shear to develop and bring the beam to failure. The existence of a minimum in the failure shearing force when the crack initiation position is changed has been reported also by Niwa[9,10] in a finite-element numerical study using cohesive rod elements perpendicular to a predetermined crack surface. Niwa fixed the shear span-to-depth ratio λ_l to 2·4 and assumed a linear crack path from the initiation point to the load point. The position for the crack initiation reported for the minimum shear resistance in his study was 0·62 and the non-dimensional shear was 0·33. These results compare fairly well with the results of the present model.

To summarise, in an RC element without stirrups, an unstable cracking process can occur when a certain load level is reached after a large crack growth. The beginning of this process may be attributable to a shear-flexural crack that becomes unstable, to a coalescence of microcracking around steel bars (depending on bonding conditions), to small inclined cracks appearing just above longitudinal reinforcement[30] or any other defect in the concrete matrix. Depending on the crack initiation position, the critical load varies, but there exists a position for which it is minimum, this minimum being identified with the so-called critical crack. This criterion is therefore assumed for computing the critical initial crack position and the collapse load unless the beam fails by flexure (steel yielding at the midspan). In fact, it can be observed that, if steel yielding takes place, the initial crack position corresponding to the minimum load is the one at the midspan. Consequently, if shear failure takes place, the steel is always in the elastic range.

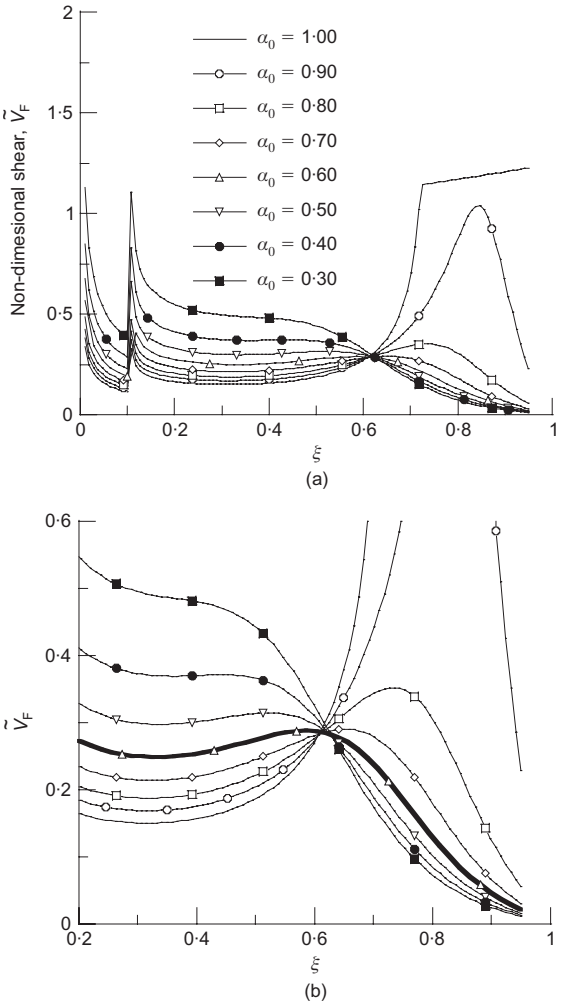

Fig. 8. (a) Non-dimensional shearing force, $\tilde{V}_F$ plotted against crack depth, ξ; (b) detail, the thick line is the curve of the minimum critical shear load

Finally, it can be observed that the presence of stirrups or reinforcement crossing the crack trajectory avoids the unstable cracking and allows for ductile behaviour of the RC element. In this case, outside the scope of the present paper, analysis of the element can be undertaken by models based on plasticity, for example strut-and-tie models.

Influence of the slenderness and the crack trajectory

As observed in the previous section, given the crack initiation position α_0 and the crack path exponent μ, each curve may present a relative maximum. Fig. 9 represents the maximum non-dimensional shearing force during crack propagation changing the location of crack initiation and the exponent of the assumed crack path. A variation is chosen in the exponent μ which defines the crack trajectory from 2 to 8, because it fits the range of experimental results. The variation in the shearing force that produces an unstable crack propagation is shown in Fig. 9(a) for a ratio λ_l equal to 2·5, and in Fig. 9(b) for a ratio λ_l equal to 5. It can be seen that, for each case, a minimum load exists as previously pointed out. It should also be noted that for all the curves obtained, the crack initiation interval where the minimum shearing force provokes diagonal tension (shear) failure is around $0{\cdot}4 < \alpha_0 < 0{\cdot}7$. This observation was made experimentally by Kim and White.[30,31] They showed that the diagonal tension failure is attributable to initiation of shear cracks near the middle of the shear span.

As can be observed in Figs 9(a) and (b), when the ratio λ_l is increased and μ remains constant, the non-dimensional shear collapse load decreases. Physically, this means that the load necessary to produce diagonal tension (shear) failure decreases when the beam slenderness increases. This is shown clearly in Figs 9(c) and (d) for exponents 4 and 6: non-dimensional shear at failure by diagonal tension decreases as the slenderness of the element increases.

Transition between failure modes

The proposed model covers steel yielding (flexural) and diagonal tension (shear) failures. It is fundamental to investigate how the transition between different failure modes is ruled according to the variation in the non-dimensional parameter N_P.

Figure 10 shows the $\tilde{V}_F$ plotted against ξ curves given by varying the brittleness number N_P from 0·2 to 1·0 and keeping the remaining parameters fixed: $\lambda_l = 2{\cdot}5$ (shear span-to-depth ratio), $\zeta = 0{\cdot}1$ (reinforcement position) and $\mu = 6{\cdot}0$ (crack path exponent).

A sketch corresponding to the crack trajectories at failure is reported at the bottom of the graphs. The horizontal dashed line represents the failure load in each case.

The model response for $N_P = 0{\cdot}2$ is shown in Fig. 10(a). When the non-dimensional shearing force $\tilde{V}_F$ reaches the value of 0·14, the flexural crack, $\alpha_0 = 1{\cdot}0$, begins its stable crack growth. An increase in the load means that this crack progresses and new cracks begin to grow in a stable way. The thick lines represent the crack's growth. The crack's growth is stable until a non-dimensional shearing force equal to 0·18 is reached, corresponding to steel yielding at the midspan. It is assumed that this value of the non-dimensional shearing force represents the flexural failure load. Thus the beam modelled in Fig. 10(a) shows a flexural failure caused by steel yielding at the midspan crack.

In Fig. 10(b) the brittleness number is increased to 0·3. The beam fails in the same way as in the previous case, by a flexural failure at the midspan crack. However, an increment of the non-dimensional shearing force at failure from 0·18 to 0·25 is observed. Comparing the crack pattern sketches it is observed that the increment in the non-dimensional shear also implies that new and deeper cracks progress through the RC element.

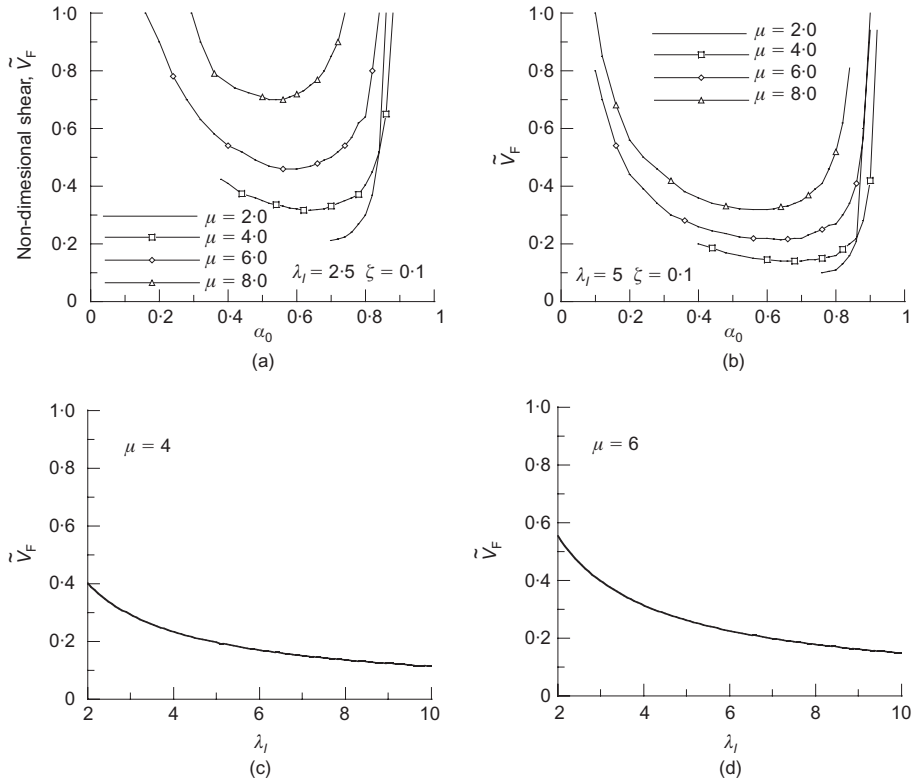

Fig. 9. Non-dimensional shearing force plotted against crack initiation position with assumptions about the crack trajectory: (a) $\lambda_l = 2{\cdot}5$; (b) $\lambda_l = 5$. Non-dimensional shearing force plotted against shear span slenderness ratio for a given crack trajectory exponent μ: (c) $\mu = 4$; (d) $\mu = 6$

If the brittleness number is increased to a value of 0·4, see Fig. 10(c), the cracking initiates and progresses similarly to the previous cases. Nevertheless, when the non-dimensional shear force reaches a value of 0·33, flexural and diagonal tension failures occur simultaneously. As observed in the above section 'Influence of the initial crack position', diagonal tension (shear) failure occurs when, after a stable crack growth, a shear crack develops unstable propagation.

For higher values of the brittleness number, flexural failure would need to occur at a higher non-dimensional shear than diagonal tension failure, so that the latter becomes the dominant failure mechanism. In Fig. 10(d) the brittleness number is set to 1·0. The load required to provoke flexural collapse for the crack situated at the midspan is 0·8, while the load at diagonal tension failure is 0·33 with a crack originating at $\alpha_0 = 0{\cdot}6$. As the assumed loading process is monotonic, the diagonal tension (shear) failure is developed before a potential flexural collapse.

Summarising, for low N_P values, cracks at the midspan (flexural cracks) need lower non-dimensional shearing forces to provoke flexural failure compared with shear cracks, situated along the middle part of the shear span, to develop diagonal shear failure. If N_P is increased, the opposite situation appears: cracks along the shear span need a lower non-dimensional shearing force to provoke beam collapse than the crack at the midspan. Thus, there is a point where the transition between these types of failure takes place.

Figure 11 shows a conceptual sketch of the failure mode transitions in RC elements without stirrups predicted by the model by varying the non-dimensional parameter N_P. The middle horizontal direction, (b) to (d), represents variations in reinforcement area whereas the diagonal directions represent variations in the scale of the beam, assuming constant reinforcement percentage, (c) to (d), or constant reinforcement area, (a) to (d).

As discussed in the first part of this section, the behaviour of the RC element is controlled by the non-dimensional parameters λ_l and N_P. As a matter of fact, if there is flexural failure (reinforcement yielding) and N_P is increased, there is a point where the failure mode changes to diagonal shear failure. This is represented in Fig. 11 with the transition from the first column, yielding failure, to the central sketch, shear failure. According to the definition, an increase in N_P can be read as

(*a*) increase in the reinforcement area, transition from (b) to (d)
(*b*) decrease in the scale with a constant reinforcement area, transition from (a) to (d)
(*c*) increase in the scale with a constant reinforcement percentage, transition from (c) to (d).

Two transition curves from the flexural to the diagonal

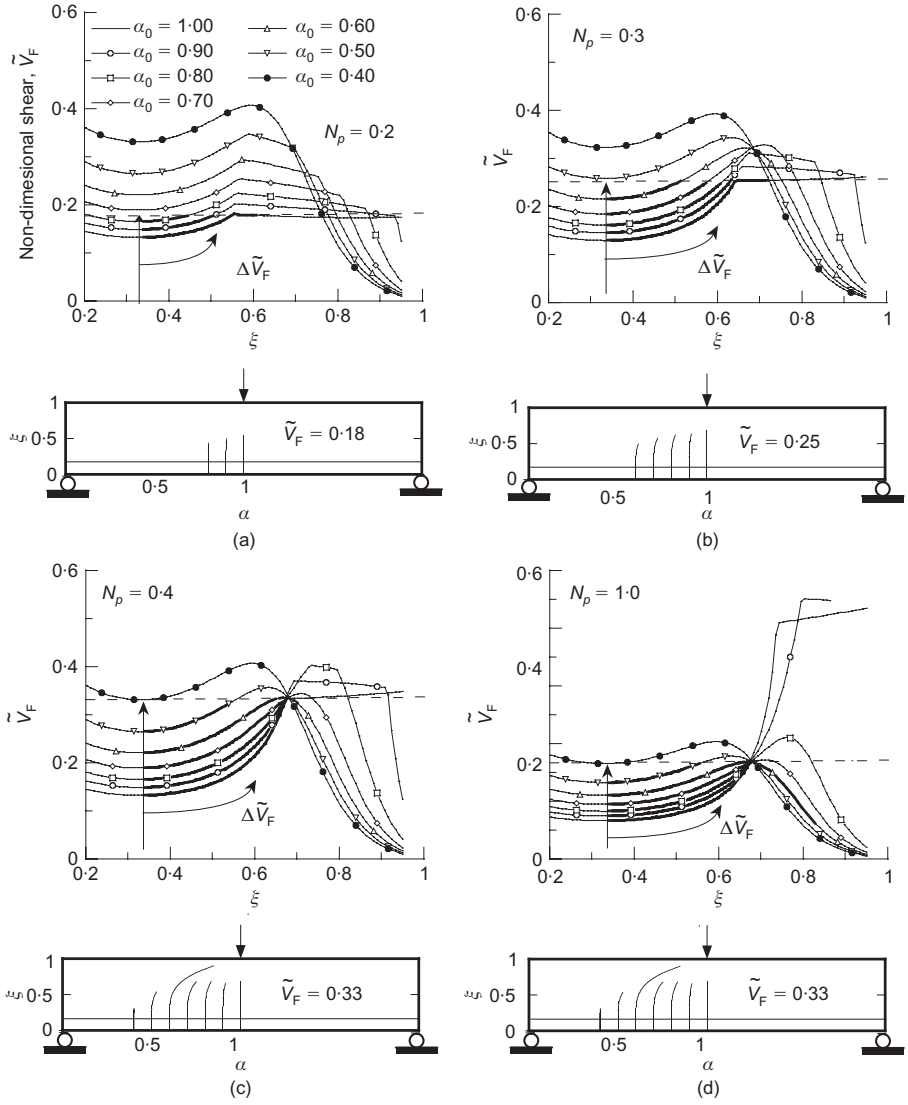

Fig. 10. Transition from flexural to diagonal tension failure in RC beams as a function of the brittleness number N_P; (a) $N_P = 0{\cdot}2$; (b) $N_P = 0{\cdot}3$; (c) $N_P = 0{\cdot}4$; (d) $N_P = 1{\cdot}0$

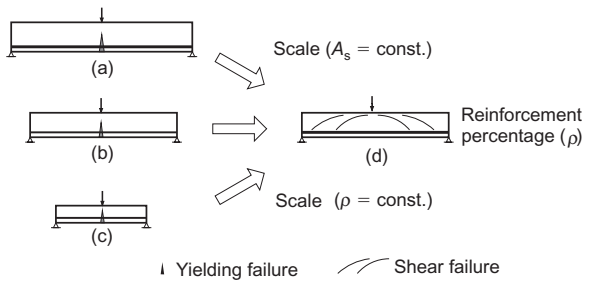

Fig. 11. Transitions between flexural and shear failures

tension (shear) failure are shown in Fig. 12. The curves are drawn for two different values of the crack trajectory exponent: $\mu = 4$ and $\mu = 6$. The two parameters controlling the model, the shear span slenderness λ_l and the brittleness number N_P, rule the transition between the two failure modes. The definition of N_P, equation (30), implies the size effect on the transition as well.

Conclusions

The current paper presents an extension of the bridged crack model to analyse flexural-shear cracks and illustrates failure mode transitions by varying the controlling non-dimensional parameters: the brittleness number N_P and the slenderness λ_l. The following conclusions can be drawn from the study.

(*a*) The model shows that diagonal tension failure is an unstable process from shear cracks and provokes the collapse of the element. It has been analytically observed that shear cracks, whose initiation point is near the middle of the shear span, need less load to develop an unstable process than

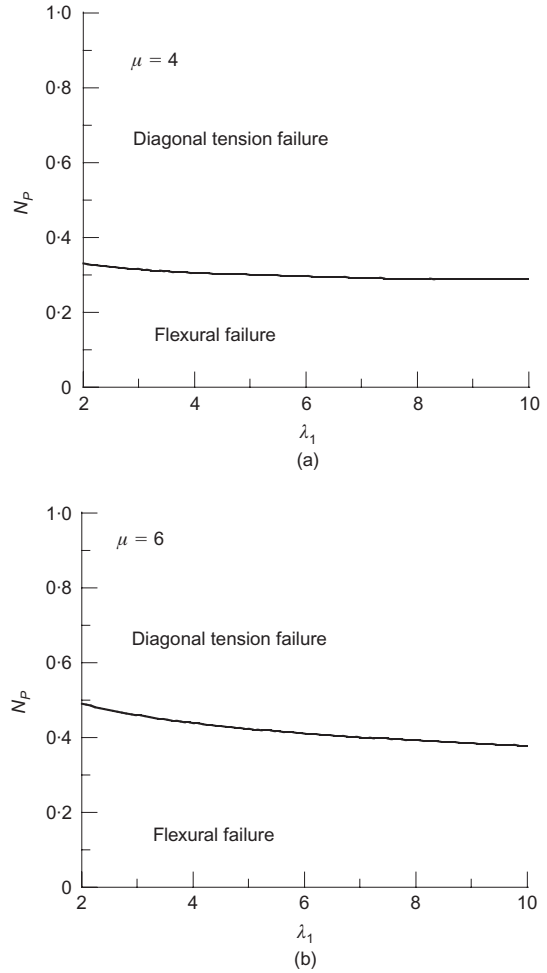

Fig. 12. Transition from flexural to diagonal tension failure in RC beams as a function of governing non-dimensional parameters N_P and λ_1: (a) $\mu = 4$; (b) $\mu = 6$

cracks near the beam midspan (flexural cracks) or cracks near the support.

(*b*) The model gives a rational explanation to the transitions between flexural and diagonal tension (shear) failures in RC beams without stirrups. Size effect in failure transitions is analysed by means of the brittleness number.[2]

(*c*) The presented analytic approach to evaluate the diagonal tension failure does not use empirical parameters, but rationally reproduces the most important trends in the behaviour of shear crack propagation through RC elements.

Possible developments of the model include a theoretical and experimental study on the choice of the crack path exponent, effect of the presence of stirrups and more technological aspects such as provisions about shear reinforcement requirements and expressions to evaluate the shear capacity of RC elements without stirrups.

Acknowledgements

The authors gratefully acknowledge the financial support of the Italian Ministry of Education, University and Research under the programme PRIN, the Ministerio de Educación y Ciencia, Spain under grant MAT2003–00843 and the Ministerio de Fomento, Spain under grant BOE305/2003. Thanks also go to the Junta de Comunidades de Castilla-La Mancha, Spain, and to the Fondo Social Europeo for the fellowships that supported the research activity.

References

1. Carpinteri A. A fracture mechanics model for reinforced concrete collapse. In *Proccedings of the I.A.B.S.E. Colloquium on Advanced Mechanics of Reinforced Concrete, Delft, The Netherlands*. International Association for Bridge and Structural Engineering, Zurich, Switzerland, 1981, pp. 17–30.
2. Carpinteri A. Stability of fracturing process in RC beams. *Journal of Structural Engineering, ASCE*, 1984, **110**, No. 3, 544–558.
3. Ruiz G. Propagation of a cohesive crack crossing a reinforcement layer. *International Journal of Fracture*, 2001, **111**, No. 3, 265–282.
4. Schlaich J., Schafer K. and Jennewein M. Toward a consistent design of structural concrete. *Journal of the Prestressed Concrete Institute*, 1987, **32**, No. 3, 74–150.
5. Vecchio F. J. and Collins M. P. The modified compression field theory for reinforced concrete elements subjected to shear. *ACI Journal*, 1986, **83**, No. 2, 219–231.
6. Collins M. P. and Mitchell D. *Prestressed Concrete Structures*. Prentice Hall, Englewood Cliffs, New Jersey, 1991.
7. Gustafsson P. J. *Fracture Mechanics Studies of Non-yielding Materials Like Concrete: Modeling of Tensile Fracture and Applied Strength Analyses*. Division of Buildings Materials, Lund Institute of Technology, Lund, Sweden, 1985, Report No. TVBM-1007.
8. Gustafsson P. J. and Hillerborg A. Sensitivity in shear strength of longitudinally reinforced concrete beams to fracture energy of concrete. *ACI Structural Journal*, 1983, **85**, No. 3, 286–294.
9. Niwa J. Size effect analyses for flexural strength of concrete beams using non linear rod element. *Proceedings of JCI*, 1993, **15**, No. 2, 75–80.
10. Niwa J. Size effect in shear of concrete beams predicted by fracture mechanics. In *CEB Bulletin d'Information No. 137: Concrete Tension and Size Effects*. Comité Euro-International du Béton (CEB), Lausanne, Switzerland, 1997, pp. 147–158.
11. Jenq Y. S. and Shah S. P. Shear resistance of reinforced concrete beams: a fracture mechanics approach. In: *Fracture Mechanics: Applications to Concrete* (Li V. and Bažant Z. P. (eds)). American Concrete Institute, Detroit, 1989, pp. 237–258.
12. So K. O. and Karihaloo B. L. Shear capacity of longitudinally reinforced beams: a fracture mechanics approach. *ACI Structural Journal*, 1993, **90**, No. 6, 591–600.
13. Karihaloo B. L. Approximate fracture mechanical approach to the prediction of ultimate shear strength of RC beams. In *Fracture Mechanics of Concrete Structures* (Wittmann F. H. (ed.)). Aedificatio Publishers, Freiburg, Germany, 1995, pp. 1111–1123.
14. Gastebled J. O. and May I. Fracture mechanics model applied to shear failure of reinforced concrete beams without stirrups. *ACI Structural Journal*, 1993, **98**, No. 2, 184–190.
15. Carpinteri A. (ed.) *Minimum Reinforcement in Concrete Members*. Number 24 in ESIS Publications. Elsevier, London, 1999.

16. Bosco C. and Carpinteri A. Fracture mechanics evaluation of minimum reinforcement in concrete structures. In *Application of Fracture Mechanics to Reinforced Concrete* (Carpinteri A. (ed.)). Elsevier, London, 1992, pp. 347–377.
17. Carpinteri A., Ferro G. and Ventura G. Size effects on flexural response of reinforced concrete elements with a non-linear matrix. *Engineering Fracture Mechanics*, 2003, **70**, No. 7, 995–1013.
18. Portela A. and Aliabadi M. H. *Crack Growth Analysis Using Boundary Elements*. Computational Mechanics Publications, Southampton, 1992.
19. Carmona J. R., Ruiz G. and del Viso J. R. Mixed-mode crack propagation through reinforced concrete. *Engineering Fracture Mechanics*, 2007, doi: 10.1016/j.engfracmech.2007.01.004.
20. Bažant Z. P. and Yu Q. Designing against size effect on shear strength of reinforced concrete beams without stirrups: I. Formulation. *Journal of Structural Engineering, ASCE*, 2005, **131**, No. 12, 1877–1885.
21. Bažant Z. P. and Yu Q. Designing against size effect on shear strength of reinforced concrete beams without stirrups: II. Verification and calibration. *Journal of Structural Engineering, ASCE*, 2005, **131**, No. 12, 1886–1897.
22. Tada H., Paris P. C. and Irwin G. R. *The Stress Analysis of Cracks Handbook*. American Society of Mechanical Engineers, New York, 2000.
23. Okamura H., Watanabe K. and Takano T. Deformation and strength of cracked member under bending moment and axial force. *Engineering Fracture Mechanics*, 1975, **7**, No. 3, 531–539.
24. RILEM TC 50-FCM. Determination of the fracture energy of mortar and concrete by means of the three-point bend test on notched beams. *Materials and Structures*, 1985, **18**, No. 4, 287–290.
25. Jenq Y. S. and Shah S. P. Determination of fracture parameters of plain concrete using three-point bend tests. *Materials and Structures*, 1990, **23**, No. 6, 457–460.
26. Abdalla H. and Karihaloo B. L. Determination of size independent specific fracture energy of concrete from three point bend and wedge splitting tests. *Magazine of Concrete Research*, 2003, **55**, No. 2, 133–142.
27. Karihaloo B. L. and Abdalla H. A simple method for determining the true specific fracture energy of concrete. *Magazine of Concrete Research*, 2003, **55**, No. 5, 471–481.
28. Bosco C., Carpinteri A. and Debernardi P. G. Minimum reinforcement in high-strength concrete. *Journal of Structural Engineering, ASCE*, 1990, **116**, No. 2, 228–236.
29. Carmona J. R. *Study of Cracking Processes in Reinforced Concrete Elements*. PhD thesis, Universidad de Castilla-La Mancha, 2006.
30. Kim W. and White R. N. Shear-critical cracking in slender reinforced concrete beams. *ACI Structural Journal*, 1999, **96**, No. 5, 757–765.
31. Kim W. and White R. N. Hypothesis for localized horizontal shearing failure mechanism of slender RC beams. *Journal of Structural Engineering, ASCE*, 1999, **125**, No. 10, 1126–1135.

Discussion contributions on this paper should reach the editor by 1 June 2008